Contents lists available at ScienceDirect

DNA Repair

journal homepage: www.elsevier.com

Proximity effects in chromosome aberration induction: Dependence on radiation quality, cell type and dose

John James Tello Cajiao[a, b, c], Mario Pietro Carante[a, b], Mario Antonio Bernal Rodriguez[c], Francesca Ballarini[a, b, *]

[a] University of Pavia, Physics Department, via Bassi 6, I-27100, Pavia, Italy
[b] INFN (Italian Institute of Nuclear Physics)-Section of Pavia, via Bassi 6, I-27100, Pavia, Italy
[c] Universidade Estadual de Campinas, Cidade Universitária Zeferino Vaz, Campinas, SP, Brazil

ARTICLE INFO

Keywords:
Chromosome aberrations
Ionizing radiation
Proximity effects
Radiation quality
Biophysical modelling
Monte Carlo simulations

ABSTRACT

It is widely accepted that, in chromosome-aberration induction, the (mis-)rejoining probability of two chromosome fragments depends on their initial distance, *r*. However, several aspects of these "proximity effects" need to be clarified, also considering that they can vary with radiation quality, cell type and dose. A previous work performed by the BIANCA (BIophysical ANalysis of Cell death and chromosome Aberrations) biophysical model has suggested that, in human lymphocytes and fibroblasts exposed to low-LET radiation, an exponential function of the form $\exp(-r/r_0)$, which is consistent with free-end (confined) diffusion, describes proximity effects better than a Gaussian function.

Herein, the investigation was extended to intermediate- and high-LET. Since the r_0 values (0.8 μm for lymphocytes and 0.7 μm for fibroblasts) were taken from the low-LET study, the results were obtained by adjusting only one model parameter, i.e. the yield of "Cluster Lesions" (CLs), where a CL was defined as a critical DNA damage producing two independent chromosome fragments. In lymphocytes, the exponential model allowed reproducing both dose-response curves for different aberrations (dicentrics, centric rings and excess acentrics), and values of F-ratio (dicentrics to centric rings) and G-ratio (interstitial deletions to centric rings). In fibroblasts, a good correspondence was found with the dose-response curves, whereas the G-ratio (and, to a lesser extent, the F-ratio) was underestimated. With increasing LET, F decreased and G increased in both cell types, supporting their role as "fingerprints" of high-LET exposure. A dose-dependence was also found at high LET, where F increased with dose and G decreased, possibly due to inter-track effects. We therefore conclude that, independent of radiation quality, in lymphocytes an exponential function can describe proximity effects at both inter- and intra-chromosomal level; on the contrary, in fibroblasts further studies (experimental and theoretical) are needed to explain the strong bias for intra-arm relative to inter-arm exchanges.

1. Introduction

Ionizing radiation impinging on living cells during the G0/G1 phase of the cell cycle can produce a variety of chromosome aberrations, mainly due to large-scale incorrect rearrangement of chromosome fragments. Since the pioneering work by Lea [1] it was clear that the involved fragments have to be created close in space, and investigating the ratios of specific aberration types can help characterizing such "proximity effects". In particular, the values of the ratio between dicentrics and centric rings ("F-ratio") observed in many experiments indicate a bias for inter-arm, intra-chromosome exchanges with respect to inter-chromosome exchanges, whereas the ratio of interstitial deletions to centric rings ("G-ratio") indicates a bias for intra-arm exchanges relative to inter-arm exchanges. In normal human cells, under the assumption of complete randomness F should be ~86 [2] and G should be ~1.2 [3], but much lower values are reported for F and larger values are reported for G. For instance, in lymphocytes exposed to low-LET radiation, F values in the range 5–20, with mean 16, have

* Corresponding author at: University of Pavia (Physics Department) and INFN-Section of Pavia Via Bassi 6, I-27100 Pavia, Italy.
Email addresses: fisk2190@gmail.com (J.J. Tello Cajiao); mariopietro.carante01@universitadipavia.it (M.P. Carante); mbernalrod@gmail.com (M.A. Bernal Rodriguez); francesca.ballarini@unipv.it (F. Ballarini)

https://doi.org/10.1016/j.dnarep.2018.02.006
Received 22 December 2017; Received in revised form 1 February 2018; Accepted 15 February 2018
Available online xxx
1568-7864/

been found [4], and G-values between 2 and 3 have been reported [5,6].

However, the interpretation of the data is complicated by the fact that both F and G can show variations depending on several factors including radiation quality, cell type and dose. Some works (e.g. [7–10] suggest that F decreases with increasing LET and can thus be considered as a "fingerprint" of high-LET exposure, whereas others (e.g. [11,12] do not show such dependence. On this issue, it is worth outlining that F is more likely to decrease with increasing LET when only a few (primary) particles cross the cell nucleus, since the presence of many particles emphasizes the so-called "inter-track effects" that lead to higher dicentric yields, and thus higher F values. As a consequence, F may be a "good" fingerprint of high-LET radiation when the doses are low and/or the cell nucleus is small, like for lymphocytes, whereas it may be a "bad" fingerprint for higher doses and/or larger cells, like fibroblasts. For the G-ratio, many works report an increase with LET; however, some other works do not show a significant increase [10]. Concerning the cell-type dependence, in lymphocytes the G-ratio tends to be smaller than in fibroblasts, for which values around 6 have been reported at low LET [13], and even higher values, around 10, have been found at high LET [14]. Furthermore, both ratios can be influenced by the considered dose levels, since inter-track effects become more significant by increasing dose.

Biophysical modelling can help clarifying the features of proximity effects, and different functions have been proposed to describe how the (mis-)rejoining probability of two chromosome fragments depends on the initial distance between the two fragment free-ends, *r*. In the framework of the Theory of Dual Radiation Action (TDRA), Kellerer and Rossi [15] suggested a function proportional to $\exp(-r^2/2\sigma^2)$ for a probability varying slowly with *r*, or alternatively a function proportional to $\exp(-r/r_0)$. The latter was applied to human fibroblasts exposed to X-rays (dose range: 2–6 Gy) by Sachs et al. [16], who compared simulated yields of different aberration categories (dicentrics, translocations, centric rings, acentric rings and eight different types of complex exchanges) with FISH experimental data. With $r_0 = 0.8\,\mu m$, a good correspondence between simulations and data was found except for an underestimation of acentric rings, which however were predicted to be about four times more frequent than centric rings, consistent with the high G-ratio generally observed in fibroblast experiments. A slowly-varying function proportional to $\exp(-r^2/2\sigma^2)$ was adopted by Holley et al. [17] and Ponomarev et al. [18]. In particular, Ponomarev et al. [18] compared their results with Giemsa data on dicentrics and centric rings in human fibroblasts exposed to gamma rays and alpha particles (dose range: 1.0–6.1 Gy for gamma rays, 0.6–2.2 Gy for alpha particles). With $\sigma = 1.0\,\mu m$, good agreement with dicentrics was found, although at the higher doses the dicentric yields were overestimated; the behavior of rings was less clear. The calculated F-ratio for γ-rays at 2 and 3 Gy, which was about 30, was substantially higher than the experimental one, which was between 6 and 7. For the G-ratio the simulations provided very high numbers, in the order of 10^3; however, a direct comparison with the data was not feasible because very small acentric rings, with size well below the experimental resolution, were also considered in the simulations.

Inverse-power laws have also been proposed: for instance, Edwards et al. [19] modelled dicentric induction in human lymphocytes applying a DSB rejoining probability of the form

$$P(r) = k/r^n \quad (1)$$

where *k* and *n* were adjustable parameters. Good agreement was found with gamma-ray data, although for alpha particles the model overestimated the data. Very interesting results have also been obtained by Sachs and co-workers [20] with their two-parameter CAS (Chromosome Aberration Simulator) model, which assumes that only (reactive) DSBs induced in the same "site" can interact, where sites are defined as intra-nuclear regions whose number is an adjustable parameter. Although the calculations underestimated the number of acentric rings, the CAS model adequately matched experimental data for many different categories of aberrations in fibroblasts exposed to gamma rays and alpha particles. Analogous results have been obtained in our previous works in the framework of the BIANCA (BIophysical ANalysis of Cell death and chromosome Aberrations) biophysical model with a step function [21], which allowed to reproduce dose-response curves for dicentrics, centric rings and excess acentric fragments, whereas underestimated the yields of interstitial deletions.

More recently [22], we have implemented both an exponential model of the form $\exp(-r/r_0)$ and a Gaussian model, which have been tested on lymphocytes and fibroblasts exposed to gamma rays (dose range: 1–4 Gy for lymphocytes, 1–6.1 Gy for fibroblasts). Both the exponential approach (with $r_0 = 0.8\,\mu m$ for lymphocytes and $r_0 = 0.7\,\mu m$ for fibroblasts) and the Gaussian one allowed to obtain a good agreement with experimental yields of Giemsa-stained dicentrics and centric rings, and thus with the F-ratio. The exponential model also allowed reproducing the yields of excess acentric fragments, whereas the Gaussian one substantially underestimated them. With both models, the calculated G-ratios for lymphocytes were in good agreement with the experimental ones, whereas for fibroblasts the simulations substantially underestimated the experimental results; however, the exponential model provided higher G-ratios than the Gaussian one. Overall, these results suggest that, at least for low-LET radiation, an exponential function describes proximity effects better than a Gaussian one. On the other hand, while for lymphocytes the exponential function allowed to reproduce both F and G, for fibroblasts it allowed to reproduce F but it underestimated G.

In the present work the investigation was extended to higher LET values. To avoid the possible introduction of biases due to inter-laboratory variations, the data for comparison were taken from the same papers considered in the previous study on low-LET radiation, i.e. from Bauchinger and Schmid [12] for lymphocytes and from Cornforth et al. [14] for fibroblasts. Like in the low-LET study, the comparison with the experimental results was performed both for dose-response curves of different aberration categories (dicentrics, centric rings and excess acentric fragments) and for F- and G-ratios. The main aspects of this approach will be reported in Section 2, whereas in Section 3 the results will be presented and discussed, as well as their possible interpretation in terms of biophysical mechanisms.

2. Materials and methods

2.1. Model assumptions and general features

The present work was performed by means of a biophysical model, implemented in the form of a Monte Carlo simulation code, that initially was specific for radiation-induced chromosomal aberrations [23–26], and later has been extended to cell death [27,28,21,29,30]. This extended version has been named BIANCA. A detailed description of the most recent version, called BIANCA II, can be found elsewhere [31–33]. The basic idea is that some DNA damage types lead to chromosome aberrations via distance-dependent mis-rejoining (or un-rejoining) of chromosome fragments, and some aberration types lead to clonogenic cell death. More specifically, the following basic assumptions have been adopted: 1) ionizing radiation induces DNA "cluster lesions" (CLs), where by definition a CL is a critical damage that produces two independent chromosome fragments; 2) distance-dependent mis-rejoining (or un-rejoining) of chromosome fragments leads to chromosomal aberrations; 3) dicentrics, rings and deletions visible under Giemsa staining lead to clonogenic cell death. A discussion on these assumptions can be found in the previous works quoted above.

Since the type(s) of damage that can be regarded as critical DNA lesions leading to chromosome aberrations is still an open question, Cluster Lesions are not characterized *a priori* at a molecular level, and the CL yield (mean number of CLs per Gy and per cell) is a parameter that is adjusted following comparisons with experimental data. According to our experience, and in agreement with the biophysical meaning of this parameter, the CL yield mainly depends on radiation quality, although it is also modulated by the target cell features. More specifically, for a given particle type the CL yield tends to increase with LET, and more CLs are induced in more radiosensitive cells. In a previous work [29], CL yields used for normal human fibroblasts have been compared with yields of DNA fragments of different sizes. The particle- and LET-dependence shown by the CL yield was found to be similar to the dependence shown by DNA fragments with size in the range 0.2–1 kbp, suggesting that a CL might be identified with a cluster of DSBs within several hundreds base-pairs. A role of DSB clustering at the kbp scale would be consistent with other available works (e.g. [34]. Interestingly, this clustering scale corresponds to the chromatin fibre level, since the amount of DNA involved in a nucleosome is about 200 bp, and there are about 1200 bp per chromatin turn.

The various CLs are distributed within the cell nucleus according to radiation track-structure. For X- and γ-rays, which are sparsely-ionizing radiation, such distribution is uniform; on the contrary, the CLs induced by a (low-energy) proton or He-ion are placed along the trajectory of the primary particle, which is represented as a segment traversing the cell nucleus. For heavier ions, some CLs are located radially with respect to the primary particle, to take into account the effects of high-energy secondary electrons.

The interaction between the various fragment free-ends is modelled as a stochastic process in which the initial distance, *r*, between two free-ends determines their probability of undergoing end-joining. As mentioned above, in previous works a step function (with cut-off distance equal to the mean distance between two adjacent chromosome territories) has been applied. Introducing a fragment un-rejoining probability (which was the second, and last, adjustable parameter), good agreement was found with experimental data on dicentrics, centric rings (and thus their ratio F) and (total) excess acentric fragments induced by different radiation qualities, whereas interstitial deletions were underestimated and terminal deletions were overestimated. It was therefore possible to reproduce the bias for inter-arm exchanges relative to inter-chromosome exchanges, but not the bias for intra-arm to inter-arm exchanges. This approach is acceptable for our cell survival studies, where the main goal is to model the total number of (lethal) aberrations. However, to allow for a deeper investigation on proximity effects, very recently [22] an exponential function of the form $\exp(-r/r_0)$ and a Gaussian function have been implemented, where the characteristic distance is the second, and last, adjustable parameter. For a detailed description of the *Geometry, Interaction* and *Scoring* modules of the code, we refer the reader to the previous work on low-LET radiation [22]; the main aspects will be reported in Section 2.2.

2.2. Simulation of the target nucleus, initial damage induction and aberration production

Like in our previous works, a lymphocyte nucleus was modelled as a 3-μm-radius sphere, whereas a fibroblast nucleus was modelled as a cylinder with elliptical base, with 4-μm height, 20-μm major axis and 10-μm minor axis. The 46 interphase chromosome territories were constructed in the same way as in [22], that is, all chromosomes were placed at random within a 3D grid consisting of 0.1-μm-side cubic voxels. Each chromosome occupied a well-defined territory and had two explicit sub-domains representing its arms.

For simulating the irradiation with protons or alpha particles, the mean number of CLs per Gy and per cell was converted into the mean number of CLs per primary particle track, based on the mean number of primary particles traversing the cell nucleus.

More specifically, assuming irradiation with a parallel beam, the mean number of primary particles traversing the nucleus, N, was calculated as

$$N = D \cdot S/(0.16 \cdot L) \quad (2)$$

where D is the absorbed dose in Gy, S is the nucleus cross-sectional area in μm^2, L is the LET in keV/μm, and 0.16 is a factor coming from the conversion of eVs into Joules, assuming a nucleus mass density of 1 g/cm^3.

The mean number of CLs per primary track was then computed as

$$CL/track = (CL \cdot cell^{-1})/N = CL \cdot Gy^{-1} \cdot cell^{-1} \cdot 0.16 \cdot L \cdot S^{-1} \quad (3)$$

For making comparisons between nucleus traversals of different lengths, it is also useful to consider the mean number of CLs per unit traversal length, which is given by

$$CL/\mu m = CL \cdot Gy^{-1} \cdot cell^{-1} \cdot 0.16 \cdot L \cdot V^{-1} \quad (4)$$

where V is the volume of the nucleus in μm^3.

For each run of the code, an actual number of nucleus traversals was extracted from a Poisson distribution, and for each traversal an actual number of CLs was extracted from another Poisson distribution. These CLs were then distributed along the segment representing the trajectory of that primary particle. After distributing all CLs in the nucleus volume, the chromosome and the chromosome-arm that were hit by each CL were identified, and the characteristics of the various chromosome fragments (length in Mbps and presence of centromere and telomeres) were recorded.

Afterwards, the code was ready to simulate the interaction between fragment free-ends according to either the exponential function or the Gaussian one. The algorithm consists of selecting two free-ends at random and deciding whether they will join or not. The possibility that finally a free-end will not undergo rejoining with any partner is automatically taken into account, because if two free-ends have been selected and their rejoining has been refused, the subsequent choice of the same pair of free-ends is forbidden. Finally, the scoring of the various aberration types is carried out. In view of comparisons with Giemsa data, chromosome fragments that had a DNA content smaller than 3 Mega-base-pair (Mbp) were not considered, because they are not visible in metaphase under Giemsa staining [35]. A discussion on the role of this value can be found in [29,22].

3. Results and discussion

3.1. Human lymphocytes

3.1.1. Proton aberration yields

Figs. 1–3 show the results obtained in this work for lymphocytes irradiated with protons of 3.5, 5.3, and 19.0 keV/μm, respectively. Each figure includes the calculated absolute yields of dicentrics (DIC), centric rings (CER) and excess acentric fragments (ACE), as well as experimental data taken from the literature [12]. Since the r_0 parameter should not depend on radiation quality, the same value used in the previous work for photons [22] was applied, i.e. $r_0 = 0.8$ μm. This choice is related to the fact that r_0, which represents the characteristic distance governing the (mis-)rejoining probability, should be mainly related to interphase chromatin organization and mobility. As shown in our previous work on low-LET radiation [22], the value of r_0 has a strong influence on the F-ratio, which increases with r_0. Some further tests performed in the present work confirmed this tendency, showing that

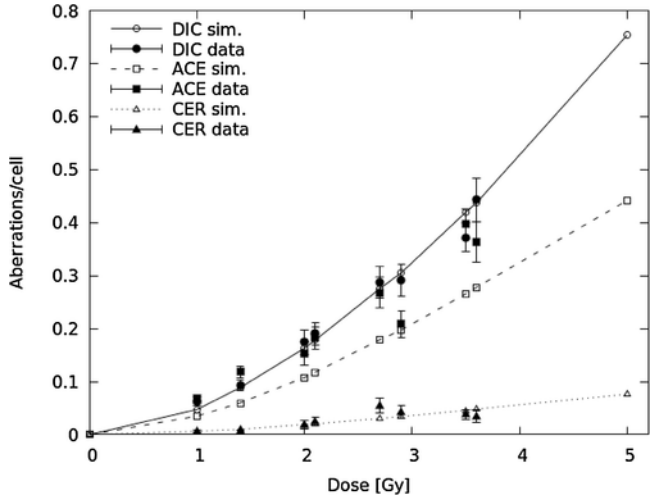

Fig. 1. Aberrations in human lymphocytes exposed to 3.5 keV/μm protons.

larger values of r_0 lead to an over-estimation of the F-ratio, whereas smaller r_0 values lead to an under-estimation of F (results not shown). The CL yield was adjusted separately for each LET value basing on the dicentric experimental yields. For all simulations, the relative uncertainty was smaller than 5%; the simulation outcomes were therefore reported without error bars, which would be smaller than the symbol size.

For protons of 3.5 keV/μm (Fig. 1), the calculated yields of both dicentrics and centric rings, and thus the F-ratio (see Section 3.1.3 below), were in good agreement with the data, since in most cases the simulation outcome was within the experimental error bar. Concerning acentrics, the simulations were systematically lower than the data, which were very similar to dicentrics. However, this was not the case neither for the photon results obtained in the previous work [22], nor for the 5.3 keV/μm results obtained in this work (see Fig. 2 below), where the dicentric yields were higher than the acentric yields, not only in the simulations but also in the data. In general, both theoretical and experimental works suggest that at low LET the yield of acentrics tends to be lower than that of dicentrics, whereas at high LET the opposite scenario occurs; this issue will be discussed in Section 3.1.2. The fact that the simulated G-ratio was consistent with the corresponding experimental value (see Section 3.1.3), suggests that the underestimation of total acentrics found at 3.5 keV/μm is mainly related to an underestimation of (large) linear fragments, rather than interstitial deletions.

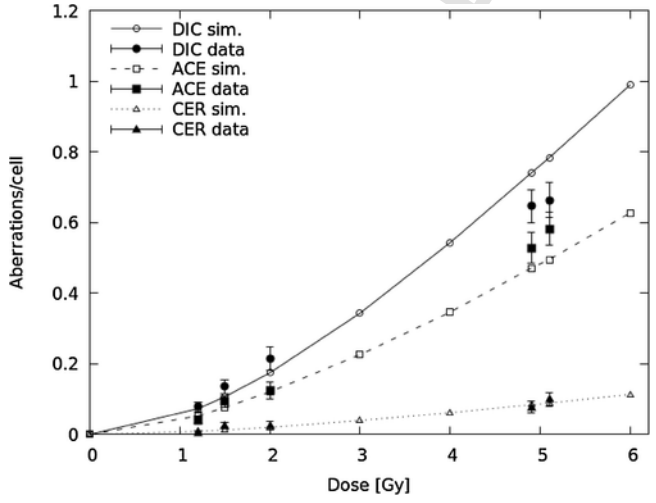

Fig. 2. Aberrations in human lymphocytes exposed to 5.3 keV/μm protons.

Empty symbols, connected by lines to guide the eye (solid line for dicentrics, dashed line for excess acentrics and dotted line for centric rings), represent simulation outcomes obtained with 0.02 CL/μm. Full symbols are experimental values taken from Bauchinger and Schmid [12]; the error bars represent one standard deviation from the mean, calculated from the raw numbers assuming Poisson statistics.

Fig. 2 shows the results obtained for protons of 5.3 keV/μm. At lower doses (up to 2 Gy), the absolute aberration yields show very good agreement with the experimental data for all three aberration categories. For the two highest doses (4.9 and 5.1 Gy), the dicentric yields were (slightly) overestimated, whereas the yields of acentric fragments were (slightly) underestimated.

Empty symbols, connected by lines to guide the eye (solid line for dicentrics, dashed line for excess acentrics and dotted line for centric rings), represent simulation outcomes obtained with 0.03 CL/μm. Full symbols are experimental values taken from Bauchinger and Schmid [12]; the error bars represent one standard deviation from the mean, calculated from the raw numbers assuming Poisson statistics.

The results obtained at 19 keV/μm are reported in Fig. 3. Concerning dicentrics, if one excludes the experimental point at 3.6 Gy, which is much lower than that at 3.7 Gy, a good correspondence between simulations and data was found, although the simulations (slightly) underestimated the data at the lower doses and (slightly) overestimated the point at the highest dose (3.7 Gy). Analogous conclusions can be drawn for acentrics if one excludes the experimental point at 1.1 Gy, which is as high as that at 1.4 Gy, and the point at 3.6 Gy, which is much lower than that at 3.7 Gy.

Empty symbols, connected by lines to guide the eye (solid line for dicentrics, dashed line for excess acentrics and dotted line for centric rings), represent simulation outcomes obtained with 0.21 CL/μm. Full symbols are experimental values taken from Bauchinger and Schmid [12]; the error bars represent one standard deviation from the mean, calculated from the raw numbers assuming Poisson statistics.

3.1.2. Alpha-particle aberration yields

Simulations were then run for 150 keV/μm alpha particles, for which the paper by Bauchinger and Schmid [12] also contains experimental data. This data set is particularly interesting because, due to the high-LET and the small nucleus cross-sectional area, especially at relatively low doses it was very unlikely that a cell was hit by more than one particle: representing a lymphocyte nucleus as a sphere with a 3-

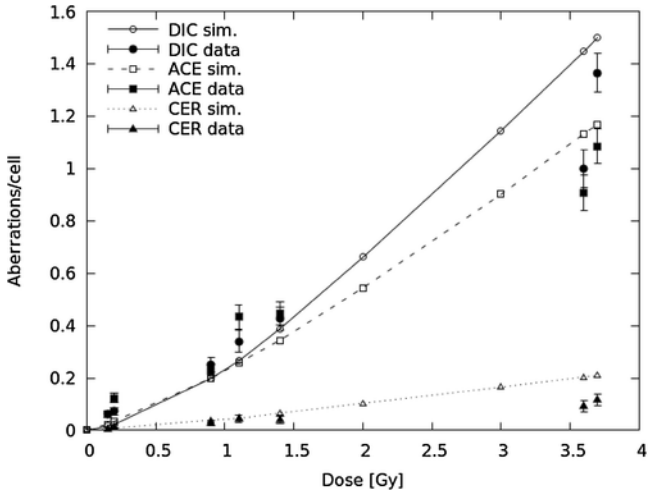

Fig. 3. Aberrations in human lymphocytes exposed to 19.0 keV/μm protons.

μm radius, even at the highest dose (1 Gy) the mean number of particle traversals is 1.2. These data thus help clarifying what happens when a single alpha particle traverses the cell nucleus, which cannot be easily derived from lymphocyte data at higher doses and/or fibroblast data, for which an inter-track action due to the presence of multiple traversals cannot be excluded. More specifically, comparing with these data allowed estimating the yield of critical DNA damages (where "critical" means severe enough to lead to chromosome aberrations) induced by an alpha particle, which at 150 keV/μm resulted to be about 1 CL/μm (see below). This is consistent with experimental results obtained by Costes et al. [36]: measuring the induction of γH2AX, ATMp and 53BP1 foci in human epithelial cells exposed to 1 GeV/amu Fe ions, which also have a LET of about 150 keV/μm, these authors found a (maximum) number of foci that was ~0.7–0.8 foci/μm. Concerning the effectiveness of a single particle traversal, further experimental data are desirable on different particle types and/or different energies, especially data obtained by microbeam irradiation, which allows delivering an exact number of particles rather than a mean number.

The results obtained with 1.06 CL/micron are reported in Fig. 4, which also shows the corresponding experimental data. Good agreement between simulations and data was found for both dicentrics and acentrics, since the discrepancies were within the experimental error in most cases. Interestingly, while at low and intermediate LET the dicentric yields were higher than the acentric yields, at 150 keV/μm the yields of acentrics became higher than those of dicentrics, both in the simulations and in the data. A cell-type dependence may also play a role, because in fibroblasts the ratio between total acentrics and dicentrics seems to be higher than in lymphocytes (see below). The interpretation of this phenomenon in terms of mechanisms is not trivial, because one would need to distinguish between terminal deletions, which are produced by a single, un-rejoined chromosome break, and interstitial deletions, which are produced by two breaks induced in the same chromosome arm. If the increase in (total) excess acentrics results to be due to an increase in interstitial deletions, then it may be explained considering that high-LET radiation, which is densely-ionizing, is more likely to induce two breaks in the same chromosome arm with respect to low-LET radiation. In some works, including that by Bauchinger and Schmid [12], all acentrics were sub-divided into linear fragments or circular fragments. However, it is not automatic that the fragments scored as linear are terminal deletions, because some fragments scored as (small) linear forms may actually be small acentric rings where the "hole" is not visible. Experimental studies making use of pan-telomeric probes, like that performed by Mestres et al. [10], can be of great help in this regard.

Concerning centric rings, the simulations were systematically higher than the data. Of course this implies that the simulated F ratio was much lower than the experimental one. This issue will be discussed in Section 3.1.3.

Empty symbols, connected by lines to guide the eye (solid line for dicentrics, dashed line for excess acentrics and dotted line for centric rings), represent simulation outcomes obtained with 1.06 CL/μm. Full symbols are experimental values taken from Bauchinger and Schmid [12]; the error bars represent one standard deviation from the mean, calculated from the raw numbers assuming Poisson statistics.

Since in our previous work the comparison between exponential and Gaussian model was specifically performed for low-LET irradiation, in this work the simulations for alpha particles were also repeated by applying the Gaussian model. Similarly to the exponential model, the yields of dicentrics and acentrics were in good agreement with the data, whereas those of centric rings overestimated the data; however, the G-ratio was lower than that found with the exponential model. The lower G-ratio may be a consequence of the fact that, at the small distances characterizing the intra-chromosomal level, the Gaussian function decreases less rapidly than the exponential one, thus leading to a less pronounced bias for intra-arm exchanges versus inter-arm exchanges.

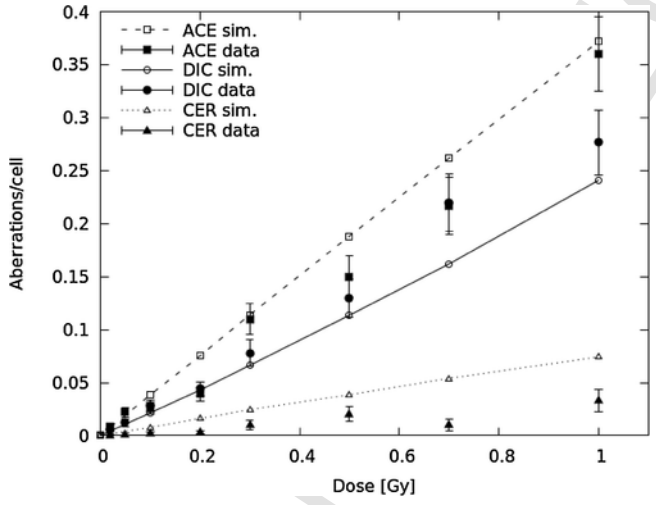

Fig. 4. Aberrations in human lymphocytes exposed to 150 keV/μm alpha particles.

3.1.3. F- and G-ratio

Table 1 summarizes the values of F-ratio and G-ratio ("Fsim." and "Gsim.", respectively) obtained with the exponential model for lymphocytes exposed to the four radiation qualities considered in this work as well as gamma rays, which have been investigated in a previous work [22]. The corresponding experimental data ("Fdata" and "Gdata", respectively), taken from Bauchinger and Schmid [12], are also reported for comparison. As already discussed in Tello et al. [22], the simulated G-ratio for gamma rays was substantially higher than the experimental one, which was even smaller than the value expected assuming randomness. However, higher values can be found in other works: for instance, a mean G-ratio of 2.84 ± 0.61 is reported in Benkhaled et al. [6], and a G-ratio of about 2 is reported in Deng et al. [5].

In the present work, the only large discrepancy was related to the F-ratio for 150 keV/μm alpha-particles; however, our results are not so inconsistent with other data reported in the literature. Using pan-centromeric and pan-telomeric probes in lymphocytes exposed to 150 keV/μm alpha-particles (dose range: 0.2–1.0 Gy), Mestres et al. [10] found a mean F-ratio of 5.47 ± 0.36. Even lower values have been observed fol-

Table 1
F-ratio (total dicentrics/total centric rings in the whole dose range) and G-ratio (total interstitial deletions/total centric rings in the whole dose range) in human lymphocytes, compared with data taken from Bauchinger and Schmid [12].

Radiation	Dose range (Gy)	*Fsim.*	*Fdata*	*Gsim.*	*Gdata*
^{137}Cs γ-rays	1.0–4.0	8.7	9.1 ± 0.8	1.6	0.9 ± 0.1
p 3.5 keV/μm	1.0–3.6	8.7	8.8 ± 1.0	1.8	1.5 ± 0.2
p 5.3 keV/μm	1.2–5.1	8.7	7.5 ± 1.0	1.8	1.5 ± 0.2
p 19.0 keV/μm	0.15–3.7	6.7	10.2 ± 1.2	2.4	2.0 ± 0.3
α 150 keV/μm	0.1–1.0	3.0	10.1n ± 1.9	3.4	3.1 ± 0.6

lowing *in vivo* alpha-particle exposure, for which Sasaki et al. [37] reported 5.0±0.3, and Tawn et al. [38] reported 4.5±2.0. Interestingly, Mestres et al. [10] noted that, when tricentrics and tetracentrics were considered as dicentric equivalents and included in the F-ratio calculation, their ratio increased to 7.16, suggesting that the inclusion of higher-order multicentrics may be significant. Also our simulations showed an increase of F if higher-order multicentrics were included (counting a tricentric as 2 dicentrics, a quadricentric as 3 dicentrics, etc.), although the increase was less pronounced than that found by Mestres et al. [10]: for instance, at 1 Gy the simulated F-ratio increased from 3.2 to 3.5. A similar trend was also found at 19 keV/μm, where, for instance, at 3.7 Gy the simulated F-ratio increased from 7.2 to 7.7 after including higher-order multicentrics.

Concerning the dependence of F and G on radiation quality, the simulations confirmed the increase of G with LET shown in various experimental works, as well as the decrease of F reported in some other works (e.g. [10,37,38]. Furthermore, the simulations at the higher LET values (19 keV/μm and 150 keV/μm) showed an increase of F with increasing dose. This is possibly related to the fact that, with increasing dose, there is an increased probability for a dicentric to be induced by two different particles (inter-track effect).

More generally, the results obtained for lymphocytes exposed to protons and alpha particles suggest that, in human lymphocytes, the dependence of the fragment (mis-)rejoining probability on the fragment initial distance can be described by an exponential function not only at low LET, as found in a previous work [22], but also at intermediate and high LET. On the contrary, the Gaussian model provided a good description of the data at high LET, but did not perform well at low LET [22]. We therefore conclude that, at least for lymphocytes, the exponential model is more realistic than the Gaussian one, independent of radiation quality.

The fact that a good agreement with the data was obtained without changing the value of r_0 is consistent with the biophysical meaning of this parameter, which should be related to the chromatin mobility features independent of radiation quality. Many authors (e.g. [39]) found that chromatin free-end mobility is mainly governed by diffusion, whereas others hypothesize an active transport mechanism. Interestingly Friedland and Kundrát [40,41], in an independent simulation work assuming free-end diffusion, found *a posteriori* that the mis-rejoining probability decreased exponentially with increasing the initial distance between the two involved DNA ends. This implies that an exponential decrease is consistent with a diffusion mechanism, at least for chromosome aberration production by Non-Homologous End Joining. Of course this does not exclude that in other repair pathways an active transport can play a role. To investigate this issue, it is desirable that further experiments are performed where the time-dependent motion of DNA free-ends is followed, e.g. by time-lapse observation of repair proteins foci. Performing these observations in different cell types which adopt different repair pathways (and/or at different cell-cycle stages where different pathways are activated), should help identifying possible scenarios where an active transport may play a role.

3.2. Human fibroblasts

In the previous work on low-LET [22], the exponential model has been also applied to human fibroblasts, comparing the simulations with experimental data on γ-ray-irradiated AG1522 cells taken from Cornforth et al. [14]. These comparisons showed a good agreement with dicentrics and rings and a reasonable agreement with total deletions; on the contrary interstitial deletions, and thus the G-ratio, were substantially underestimated. This suggests that, at least for low-LET radiation, an exponential model of the form $\exp(-r/r_0)$ can reproduce the proximity bias for inter-arm exchanges with respect to inter-chromosome exchanges not only in lymphocytes but also in fibroblasts. However, different from lymphocytes, in fibroblasts such exponential model underestimates the bias for intra-arm versus inter-arm exchanges. A Gaussian model provided a worse performance, since it allowed obtaining good agreement for dicentrics and rings, and thus for the F-ratio, but substantially underestimated total acentrics.

3.2.1. Alpha-particle aberration yields

In this work we extended the investigation to high-LET radiation, taking the data for comparison from the same paper considered for photons [14], which also reports data on AG1522 cells exposed to 116 keV/μm alpha particles. Fig. 5 displays the outcomes obtained by applying the exponential model with $r_0 = 0.7$ μm (the same value used for photons) and 0.47 CL/μm; the data reported in Cornforth et al. [14] are also shown. Analogous to what found for photons, the simulations compare reasonably well with the data both for dicentrics and for excess acentrics. On the contrary the experimental rings were overestimated, implying that the simulated F-ratio was smaller than the experimental one (see Section 3.2.2).

The results obtained with the exponential model for AG1522 cells exposed to high-LET radiation thus confirmed the main features of those obtained at low LET, since the simulations were in agreement with the data for dicentrics and total acentrics, whereas interstitial deletions were underestimated. Furthermore, at high LET the experimental yield of rings was overestimated. This implied that, at high LET, the G-ratio and the F-ratio were both underestimated. Reducing the value of r_0 allowed to obtain higher values for G but even lower values for F: for instance, using $r_0 = 0.5$ μm, at 2.2 Gy the G-ratio increased from 5.2 to 6.4, but the F-ratio decreased from 3.3 to 2.6.

Empty symbols, connected by lines to guide the eye (solid line for dicentrics, dashed line for excess acentrics and dotted line for centric rings), represent simulation outcomes obtained with 0.47 CL/μm. Full symbols are experimental values taken from Cornforth et al. [14]; the error bars represent one standard deviation from the mean, calculated from the raw numbers assuming Poisson statistics.

Since for α-particle-irradiated lymphocytes the performance of the Gaussian model was not very different from that of the exponential model, also for α-irradiated fibroblasts simulations were run applying the Gaussian model. Like at low LET [22], the exponential model and the Gaussian one behaved rather similarly for dicentrics and centric rings (and thus for the F-ratio), but the exponential model was closer to the data both for total acentrics and for the G-ratio (results not shown).

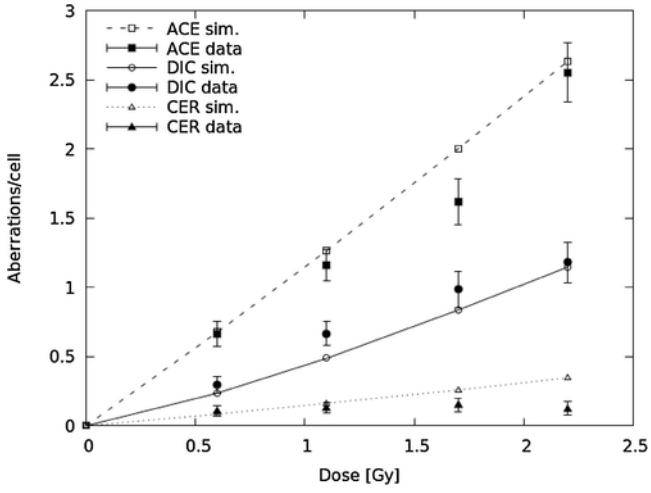

Fig. 5. Aberrations in human fibroblasts exposed to 116 keV/μm alpha particles.

3.2.2. F- and G-ratio

Table 2 reports the values of F-ratio and G-ratio ("Fsim" and "Gsim", respectively) obtained with the exponential model for fibroblasts exposed to 116 keV/μm alpha-particles as well as gamma rays, which have been investigated in a previous work [22]. The corresponding experimental data ("Fdata" and "Gdata", respectively), taken from Cornforth et al. [14], are also reported for comparison. As mentioned above, a major discrepancy is related to an underestimation of G for both radiation types, and possibly an underestimation of F for alpha particles.

It is interesting to note that also in the simulations G increased with LET, consistent with the data. Concerning the dose-dependence, in the simulations F increased with dose, like for alpha-particle-irradiated lymphocytes; furthermore, G significantly decreased with increasing dose. Possible explanations for such a decrease of G, which was found for fibroblasts but not for lymphocytes, might include a more pronounced role of inter-track effects, related to the higher number of particles involved: while in lymphocytes the (mean) fluence at the highest dose was 0.04 particles/μm^2, in fibroblasts it was 0.12 particles/μm^2.

The substantial underestimation of the G-ratio suggests that even an exponential function of the form $\exp(-r/r_0)$ is not sufficient for reproducing the large bias for intra-arm exchanges to inter-arm exchanges observed in fibroblasts, which deserves further investigation in the future. The fact that in fibroblasts such bias seems to be more pronounced than in lymphocytes might be related to many biological factors, including not only a reduced mobility of chromatin [39] but also its 3D organization in the cell nucleus during interphase, as well as the dimensions of the various chromosome territories. Since the volume of fibroblast nuclei is much larger than that of human lymphocyte nuclei, the (mean) volume of a chromosome territory is much larger in fibroblasts than in lymphocytes. Assuming that, after a given time interval, a chromosome free-end induced in a fibroblast has travelled a similar distance as a free-end induced in a lymphocyte, then for fibroblasts a free-end initially induced in a given chromosome arm may be more likely to stay within that arm domain, and possibly join with another free-end induced in the same arm, thus giving rise to an interstitial deletion (or a paracentric inversion). On the contrary, for lymphocytes a free-end initially induced in a given arm may have a higher probability of reaching the domain occupied by the other arm and joining with a free-end induced there, thus producing an inter-arm exchange like a centric ring (or a pericentric inversion). This may explain why the values of G-ratio experimentally observed in fibroblasts tend to be higher than in lymphocytes, and why an exponential function allows to reproduce the G-ratio in human lymphocytes but underestimates it in human fibroblasts.

More generally, these findings support a scenario where the intrinsic mobility properties of chromatin free-ends have a strong influence on the distance-dependence of the (mis-)rejoining probability. In turn, such properties might be related to interphase chromatin organization, including the existence of attachment points to the nuclear matrix: one possibility is that, after a (complex) DSB has been induced, the maximum distance that a free-end can travel is given by the length of the chromatin loop between two subsequent attachment points. For instance, considering a loop having a size of 50–200-kbp (e.g. [42], and assuming that each 1.2-kpb structure corresponds to 10 nm, one would obtain a distance of ~0.4–1.6 μm, which is consistent with the characteristic distance for the mis-rejoining probability found in this and other works.

4. Summary and conclusions

By means of the BIANCA biophysical model, a previous study on proximity effects in human lymphocytes and fibroblasts exposed to low-LET radiation was extended to intermediate and high LET. The results suggested that, independent of radiation quality, in lymphocytes an exponential function of the form $\exp(-r/r_0)$ can describe both the bias for inter-arm exchanges relative to inter-chromosome exchanges (F-ratio), and that for intra-arm to inter-arm exchanges (G-ratio). On the contrary, in fibroblasts this function can describe the former bias but underestimates the latter. This might be related to differences in chromatin mobility and/or in the 3D organization of the cell nucleus during interphase, as well as in the dimensions of the various chromosome territories. The fact that, with increasing LET, F decreased and G increased in both cell types, supports their possible role as "fingerprints" of high-LET exposure. A dose-dependence was also observed at high LET, where F increased with dose in both cell types, whereas G decreased in fibroblasts but not in lymphocytes. Table 3 reports a schematic overview of the main findings related to the F- and G-ratios, including the agreement with experimental data, the dose-dependence and the LET-dependence.

In light of these findings, further studies, including chromosome aberration experiments with pan-telomeric probes and time-lapse observation of repair protein foci, are desirable to better characterize and quantify these effects. Furthermore, it is important that in the aberration studies the specific conditions (e.g. dose-range, cell type and scoring criteria, including those adopted for higher-order multicentrics) are reported and taken into account when interpreting the results.

Conflict of interest

The authors declare that there are no conflicts of interest.

Acknowledgements

This work was supported by the Italian Institute of Nuclear Physics [projects "ETHICS" and "MC-INFN/FLUKA"] and the Conselho Nacional para o Desenvolvimento Científico e Tecnológico (CNPq) in Brazil [grant number 306775/2015-8]. We also thank the Reviewers, in particular Reviewer #1, whose comments helped improving the presentation of the work.

Table 2
F-ratio (total dicentrics/total centric rings in the whole dose range) and G-ratio (total interstitial deletions/total centric rings in the whole dose range) in AG1522 human fibroblasts, compared with data taken from Cornforth et al. [14].

Radiation	Dose-range (Gy)	*Fsim.*	*Fdata*	*Gsim.*	*Gdata*
^{137}Cs γ-rays	1.0–6.1	5.1	5.3 ± 0.6	2.2	6.8 ± 0.8
α 116 keV/μm	0.6–2.2	3.2	5.7 ± 1.0	5.5	10.3 ± 1.8

Table 3
Agreement with data and dependence on LET and dose for the F-ratio and the G-ratio.

Cell type	Agreement with data		Dose dependence		LET dependence	
	F	G	F	G	F	G
lymph, low-LET	OK	OK	–	–	↓	↑
lymph, high-LET	OK/under	OK	↑	–		
fibro, low-LET	OK	under	–	–	↓	↑
fibro, high-LET	∼OK	under	↑	↓		

lymph = lymphocytes; fibro = fibroblasts.
OK = good agreement; under = underestimation; OK/under = agreement for some data, underestimation for others.
– = no significant dependence; ↑ = increasing; ↓ = decreasing.

References

[1] D.E. Lea, Actions of Radiations on Living Cells, Univ. Press Cambridge, 1946.
[2] R.K. Sachs, A.M. Chen, D.J. Brenner, Review: proximity effects in the production of chromosome aberrations by ionizing radiation, Int. J. Radiat. Biol. 71 (1997) 1–19.
[3] R.K. Sachs, D.J. Brenner, A.M. Chen, P. Hahnfeldt, L.R. Hlatky, Intra-arm and interarm chromosome intrachanges: tools for probing the geometry and dynamics of chromatin, Radiat. Res. 148 (1997) 330–340.
[4] L.R. Hlatky, R.K. Sachs, P. Hahnfeldt, The ratio of dicentrics to centric rings produced in human lymphocytes by acute low-LET radiation, Radiat. Res. 129 (1992) 304–308.
[5] W. Deng, D.P. Morrison, K.L. Gale, J.N. Lucas, A comparative study on potential cytogenetic fingerprints for radiation LET in human lymphocytes, Int. J. Radiat. Biol. 76 (2000) 1589–1598.
[6] L. Benkhaled, L. Barrios, M. Mestres, M.R. Caballin, M. Ribas, J.F. Barquinero, Analysis of gamma-rays induced chromosome aberrations: a fingerprint evaluation with a combination of pan-centromeric and pan-telomeric probes, Int. J. Radiat. Biol. 82 (2006) 869–875.
[7] J. Pohl-Rüling, P. Fischer, D.C. Lloyd, A.A. Edwards, A.T. Natarajan, G. Obe, K.E. Buckton, N.O. Bianchi, P.P. van Buul, B.C. Das, Chromosomal damage induced in human lymphocytes by low doses of D-T neutrons, Mutat. Res. 173 (1986) 267–272.
[8] D.J. Brenner, R.K. Sachs, Chromosomal fingerprints of prior exposure to densely ionizing radiation, Radiat. Res. 140 (1994) 134–142.
[9] F. Ballarini, A. Ottolenghi, Chromosome aberrations as biomarkers of radiation exposure: modelling basic mechanisms, Adv. Space Res. 31 (2003) 1557.
[10] M. Mestres, M.R. Caballin, E. Schmid, G. Stephan, R. Sachs, L. Barrios, J.F. Barquinero, Analysis of α-particle induced chromosome aberrations in human lymphocytes, using pan-centromeric and pan-telomeric probes, Int. J. Radiat. Biol. 80 (2004) 737–744.
[11] J.R.K. Savage, D.G. Papworth, Comment on the ratio of chromosome-type dicentric interchanges to centric rings for track-clustered compared with random breaks, Radiat. Res. 146 (1996) 236–240.
[12] M. Bauchinger, E. Schmid, LET dependence of yield ratios of radiation-induced intra- and interchromosomal aberrations in human lymphocytes, Int. J. Radiat. Biol. 74 (1998) 17–25, https://doi.org/10.1080/095530098141681.
[13] M.C. Muhlmann-Diaz, J.S. Bedford, Comparison of gamma-ray-induced chromosome ring and inversion frequencies, Radiat. Res. 143 (1995) 175–180, https://doi.org/10.2307/3579154.
[14] M.N. Cornforth, S.M. Bailey, E.H. Goodwin, Dose responses for chromosome aberrations produced in noncycling primary human fibroblasts by alpha particles, and by gamma rays delivered at sublimiting low dose rates, Radiat. Res. 158 (2002) 43–53, https://doi.org/10.1667/0033-7587158.
[15] A.M. Kellerer, H.H. Rossi, A generalized formulation of dual radiation action, Radiat. Res. 75 (1978) 471–488, https://doi.org/10.2307/3574835.
[16] R.K. Sachs, D. Levy, A.M. Chen, P.J. Simpson, M.N. Cornforth, E.A. Ingerman, P. Hahnfeld, L.R. Hlatky, Random breakage and reunion chromosome aberration formation model; an interaction-distance version based on chromatin geometry, Int. J. Radiat. Biol. 76 (2000) 1579–1588.
[17] W.R. Holley, I.S. Mian, S.J. Park, B. Rydberg, A. Chatterjee, A model for interphase chromosomes and evaluation of radiation-induced aberrations, Radiat. Res. 158 (2002) 568–580.
[18] A.L. Ponomarev, K. George, F.A. Cucinotta, Computational model of chromosome aberration yield induced by high- and low-LET radiation exposures, Radiat. Res. 177 (2012) 727–737, https://doi.org/10.1667/RR2659.1.
[19] A.A. Edwards, V.V. Moiseenko, H. Nikjoo, Modelling of DNA breaks and the formation of chromosome aberrations, Int. J. Radiat. Biol. 66 (1994) 633–637.
[20] A.M. Chen, J.N. Lucas, P.J. Simpson, C.S. Griffin, J.R.K. Savage, D.J. Brenner, L.R. Hlatky, R.K. Sachs, Computer simulation of data on chromosome Aberrations produced by x rays or alpha particles and detected by fluorescence In situ hybridization, Radiat. Res. 148 (1997) S93–S101.
[21] F. Ballarini, S. Altieri, S. Bortolussi, M. Carante, E. Giroletti, N. Protti, The BIANCA model/code of radiation-induced cell death: application to human cells exposed to different radiation types, Radiat. Environ. Biophys. 53 (2014) 525–533, https://doi.org/10.1007/s00411-014-0537-6.
[22] J.J. Tello Cajiao, M.P. Carante, M.A. Bernal Rodriguez, F. Ballarini, Proximity effects in chromosome aberration induction by low-LET ionizing radiation, DNA Repair 58 (2017) 38–46.
[23] A. Ottolenghi, F. Ballarini, M. Biaggi, Modelling radiation-induced biological lesions: from initial energy depositions to chromosome aberrations, Radiat. Environ. Biophys. 38 (1999) 1–13, https://doi.org/10.1007/s004110050132.
[24] A. Ottolenghi, F. Ballarini, M. Biaggi, Modelling chromosomal aberration induction by ionising radiation: the influence of interphase chromosome architecture, Adv. Space Res. 27 (2001) 369–382, https://doi.org/10.1016/S0273-1177(01)00004-7.
[25] F. Ballarini, A. Ottolenghi, A model of chromosome aberration induction and chronic myeloid leukaemia incidence at low doses, Radiat. Environ. Biophys. 43 (2004) 165–171, https://doi.org/10.1007/s00411-004-0246-7.
[26] F. Ballarini, A. Ottolenghi, A model of chromosome aberration induction: applications to space research, Radiat. Res. 164 (2005) 567–570, https://doi.org/10.1667/RR3365.1.
[27] F. Ballarini, From DNA radiation damage to cell death: theoretical approaches, J. Nucleic Acids 2010 (2010) e350608, https://doi.org/10.4061/2010/350608.
[28] F. Ballarini, S. Altieri, S. Bortolussi, E. Giroletti, N. Protti, A model of radiation-induced cell killing: insights into mechanisms and applications for hadron therapy, Radiat. Res. 180 (2013) 307–315.
[29] M.P. Carante, S. Altieri, S. Bortolussi, I. Postuma, N. Protti, F. Ballarini, Modeling radiation-induced cell death: role of different levels of DNA damage clustering, Radiat. Environ. Biophys. 54 (2015) 305–316, https://doi.org/10.1007/s00411-015-0601-x.
[30] M.P. Carante, F. Ballarini, Calculating variations in biological effectiveness for a 62 MeV proton beam, Front. Oncol. 6 (2016) 76, https://doi.org/10.3389/fonc.2016.00076.
[31] F. Ballarini, M.P. Carante, Chromosome aberrations and cell death by ionizing radiation: evolution of a biophysical model, Radiat. Phys. Chem. 128 (2016) 18–25, https://doi.org/10.1016/j.radphyschem.2016.06.009.
[32] M.P. Carante, F. Ballarini, Modelling cell death for cancer hadrontherapy, AIMS Biophys. 4 (2017) 465–490, https://doi.org/10.3934/biophy.2017.3.465.
[33] A. Testa, F. Ballarini, U. Giesen,, O. Monteiro Gil, M.P. Carante, F. Langner, H. Rabus, V. Palma, M. Pinto, C. Patrono, Analysis of radiation-induced chromosomal aberrations on cell-by-cell basis after 4He-ion microbeam irradiation: experimental data and simulations, Radiat. Res. (2018), in press.
[34] B. Rydberg, L. Heilbronn, W.R. Holley, M. Loebrich, C. Zeitlin, A. Chatterjee, P.K. Cooper, Spatial distribution and yield of DNA double-strand breaks induced by 3–7 MeV helium ions in human fibroblasts, Radiat. Res. 158 (2002) 32–42.
[35] M.N. Cornforth, J.S. Bedford, A quantitative comparison of potentially lethal damage repair and the rejoining of interphase chromosome breaks in low passage normal human fibroblasts, Radiat. Res. 111 (1987) 385–405, https://doi.org/10.2307/3576926.
[36] S.V. Costes, A. Ponomarev, J.L. Chen, D. Nguyen, F.A. Cucinotta, M.H. Barcellos-Hoff, Image-based modeling reveals dynamic redistribution of DNA damage into nuclear sub-domains, PLoS Comput. Biol. 3 (2007) e155, https://doi.org/10.1371/journal.pcbi.0030155.
[37] M.S. Sasaki, T. Takatsuji, Y. Ejima, S. Kodama, C. Kido, Chromosome aberration frequency and radiation dose to lymphocytes by alpha-particles from internal deposit of Thorotrast, Radiat. Environ. Biophys. 26 (1987) 227–238.
[38] E.J. Tawn, J.W. Hall, G.B. Schofield, Chromosome studies in plutonium workers, Int. J. Radiat. Biol. 47 (1985) 599–610.
[39] B. Jakob, J. Splinter, G. Taucher-Scholz, Positional stability of damaged chromatin domains along radiation tracks in mammalian cells, Radiat. Res. 171 (2009) 405–418.
[40] W. Friedland, P. Kundrát, Chromosome aberration model combining radiation tracks, chromatin structure, DSB repair and chromatin mobility, Radiat. Prot. Dosim. 166 (2015) 71–74, https://doi.org/10.1093/rpd/ncv174.
[41] W. Friedland, P. Kundrát, Track structure based modelling of chromosome aberrations after photon and alpha-particle irradiation, Mutat. Res. – Genet. Toxicol. Environ. Mutagen. 756 (2013) 213–223, https://doi.org/10.1016/j.mrgentox.2013.06.013.
[42] S.V. Razin, O.V. Iarovaia, N. Sjakste, T. Sjakste, L. Bagdoniene, A.V. Rynditch, E.R. Eivazova, M. Lipinski, Y.S. Vassetzky, Chromatin domains and regulation of transcription, J. Mol. Biol. 369 (2007) 597–607.